

POSITION SENSITIVE PROPORTIONAL COUNTER SOFT X-RAY OBSERVATIONS OF SEYFERT 2 GALAXIES

T. J. TURNER,¹ C. M. URRY,² AND R. F. MUSHOTZKY³

Laboratory for High Energy Astrophysics, NASA/Goddard Space Flight Center, Greenbelt, MD 20771

Received 1993 March 10; accepted 1993 June 10

ABSTRACT

We present the results from *ROSAT* PSPC soft X-ray (0.1–2.0 keV) observations of six Seyfert 2 galaxies, chosen from the brightest Seyfert 2's detected with the *Einstein* Imaging Proportional Counter. All of the targets were detected with the *ROSAT* PSPC. Spatial analysis shows that the source density within a few arcminutes of each Seyfert 2 galaxy is a factor of ~ 8 higher than in the rest of the inner field of view of the PSPC images. In NGC 1365 it appears that the serendipitous sources may be X-ray binary systems in the host galaxy. The proximity of the serendipitous sources, typically within a few arcminutes of the target Seyfert 2, means that previous X-ray observations of the Seyfert 2 galaxies have been significantly contaminated, and that source confusion is important on a spatial scale of $\sim 1'$. Some spectra, most notably Mrk 3 and NGC 1365, indicate the presence of a high equivalent width soft X-ray line blend consistent with unresolved iron L and oxygen K emission.

Subject headings: galaxies: Seyfert — X-rays: galaxies

1. INTRODUCTION

The first X-ray all-sky surveys found that although Seyfert 1 galaxies were strong X-ray emitters, Seyfert 2's were generally not detected (Elvis et al. 1978; Tananbaum et al. 1978). When the *Einstein* Observatory telescope made fainter X-ray fluxes accessible, soft X-rays were seen from some Seyfert 2 galaxies, but the implied X-ray luminosities were generally two or more orders of magnitude smaller than those of Seyfert 1 galaxies of comparable optical magnitude (Kriss, Canizares, & Ricker 1980).

In many Seyfert 1 galaxy hard X-ray spectra, low-energy turnovers implied large absorbing column densities of cold material ($N_{\text{H}} \geq 10^{22}$ atoms cm^{-2}) along the line of sight to the X-ray source. This suggested that obscuration might cause Seyfert 2 galaxies to be faint in X-rays, as did the observation that Seyfert 2's had relatively greater infrared dust emission compared to Seyfert 1's (Rowan-Robinson 1977), although it seemed puzzling that the weak continuum emission seen in some Seyfert 2's was not heavily reddened (Koski 1978). Based on the optical, infrared, and soft- and hard-X-ray properties of a sample of active galaxies, Lawrence & Elvis (1982) concluded that obscuration in or around the broad emission-line region, arranged in a flattened configuration, plays an important role in the optical classification of Seyfert galaxies. This asymmetry implied that orientation was the likely link between Seyfert 1 and Seyfert 2 galaxies, with nuclear continuum and broad emission lines escaping only in certain directions.

Direct evidence for the link was found by Antonucci & Miller (1985), who detected broad, Seyfert 1-like emission lines in the polarized optical spectrum of the Seyfert 2 galaxy NGC 1068. The polarization is almost certainly caused by scattering, probably by electrons since it is wavelength independent (the UV is similarly polarized; Code et al. 1991; Kinney et al. 1991). The weakness of the broad lines in the total-light spectrum

means the broad-line region is hidden from direct view by obscuring material. Thus NGC 1068 seems to be a Seyfert 1 with obscuring material, perhaps a torus, along the line of sight. Scattered light from the hidden nuclear region should be apparent at all wavelengths, just reduced in strength by about two orders of magnitude (hence the weak, unreddened optical continuum sometimes seen in Seyfert 2's). Similar polarized Seyfert 1-like emission has now been seen in a number of Seyfert 2 galaxies (Miller & Goodrich 1990; Tran, Miller, & Kay 1992), implying that the torus model may be appropriate to Seyfert 2's as a class.

Subsequent X-ray observations generally supported this picture. *Ginga* observations of the Seyfert 2 galaxy Mrk 3 showed a hard X-ray spectrum with a flat power law (photon index, $\Gamma \sim 1.5$) and high absorbing column density ($N_{\text{H}} \sim 10^{23}$ cm^{-2} ; Awaki et al. 1990). Iron K lines of very high equivalent width (~ 1 keV), expected because the equivalent width of the line is measured against the scattered continuum rather than the ionizing continuum (Krolik & Kallman 1987; Band et al. 1990), were seen in the *Ginga* spectra of NGC 1068 and Mrk 3 (Koyama et al. 1989). BBXRT spectra of the same two Seyferts also showed heavily absorbed, flat, hard X-ray spectra, and strong iron K emission lines, plus an unabsorbed steep soft excess plus and a broad soft X-ray emission feature at ~ 1 keV that is thought to be a blend of iron L and oxygen emission (Marshall et al. 1991).

There remain some questions about the unified model for Seyfert galaxies and about the X-ray emission in particular. Continuum variability characteristic of an active Seyfert 1 nucleus must be smeared out in time for Seyfert 2's (as the observed radiation is hypothesized to be seen after scattering). In particular, variations faster than the light-crossing time of the scattering volume (a few years for NGC 1068) should not be seen in the soft X-ray flux, which must be scattered since the direct path is obscured. Thus the observation of fast variability in an IPC observation of Mrk 78 (Urry et al. 1986) posed a problem for the unified model. Another problem is that the prototypical Seyfert 2-as-hidden-Seyfert 1, NGC 1068, has a very steep soft X-ray spectrum (Monier & Halpern 1987) com-

¹ Code 668; also with Universities Space Research Association.

² Space Telescope Science Institute, 3700 San Martin Drive, Baltimore, MD 21218.

³ Code 666.

pared to the average soft X-ray spectrum of Seyfert 1's (Kruper, Urry, & Canizares 1991), although it also has a flat hard X-ray component (Elvis & Lawrence 1988). If the soft X-rays are indeed scattered nuclear X-rays, then the Seyfert 1 and Seyfert 2 spectra should be identical. With the exception of NGC 1068, individual Seyfert 2 galaxies were too faint in X-rays to be studied spectroscopically with the *Einstein* IPC; their summed spectra look quite unlike NGC 1068, but within large uncertainties look roughly like Seyfert 1 spectra (Kruper et al. 1991). The existence of soft excess components to the spectra of Seyfert 1's (Urry et al. 1989; Turner & Pounds 1989) complicate the comparison of Seyfert 1 and 2 X-ray spectra.

Using the greater sensitivity and higher spectral resolution of the *ROSAT* PSPC is an obvious way to address these issues. We chose a sample of Seyfert 2 galaxies known to be relatively bright in soft X-rays from previous *Einstein* IPC observations. The six approved targets are listed in Table 1, while count rates are listed in Table 2. The observations are described in more detail in § 2. Our study had three goals. First, we looked for evidence of extended emission, particularly in the closest objects, such as might be expected if Seyfert 2's have soft X-ray excesses due to hot gas in the narrow line region (cf. NGC 1068; Wilson et al. 1992). The spatial analysis presented in § 3.1 shows that earlier X-ray observations of these Seyferts have been contaminated significantly by previously unresolved nearby sources. Second, § 3.2 describes the time variability. Third, the spectral characteristics of Seyfert 2's, including continuum shape, absorption, and line emission, are described in § 3.3. These can be compared to samples of Seyfert 1's proposed separately and reported elsewhere (Turner, George, & Mushotzky 1993). Notes on individual objects are given in § 4. Our results are discussed in § 5, and the conclusions summarized in § 6.

2. THE OBSERVATIONS

The data reported here are from observations carried out using the *ROSAT* X-Ray Telescope (Truemper 1983) with the Position Sensitive Proportional Counter PSPC-B in the focal plane (Pfeffermann et al. 1986). The PSPC at the focus of the X-ray telescope provides a bandpass of ~ 0.1 – 2.4 keV over a 2° diameter field of view. The energy resolution of the PSPC detector is given by $\Delta E/E = 0.43 (E/0.93)^{-0.5}$ (FWHM), where E is in keV. The on-axis spatial resolution is $\sim 25''$ (FWHM) for the full bandpass (Hasinger et al. 1992). During these observations a slow “wobble” of the spacecraft was carried out, moving the telescope pointing direction back and forth by several arcminutes on a timescale of several minutes. This was done to prevent shadowing of X-ray sources behind the coarse

wire grid which forms part of the PSPC detector window. The PSPC background count rate is very low. The background components are the cosmic-ray-induced particle background, scattered solar X-rays, and the diffuse X-ray background.

Table 1 shows an observing log for the *ROSAT* observations. The exposure times listed in Table 1 are after the data had been screened for bad observation intervals (bad aspect solution or unusually high background rates). The accumulated PSPC counts tabulated are in pulse invariant (PI) channels 12–200 inclusive and are background subtracted. Standard Analysis Software System (SASS) processing version numbers are provided in Table 1 for each observation presented. These sources were all observed close to the center of the PSPC field of view.

3. THE DATA ANALYSIS

3.1. Spatial Analysis

3.1.1. Procedure

Analysis of the PSPC point-spread function has shown that the softest counts suffer a “ghost imaging” effect. The manifestation of this is that the association of positions of very soft events can be incorrect in a way which is not predictable (making a valid parameterization of the point spread function currently impossible at the softest energies). This effect is strongest below channel 15, but in high signal-to-noise ratio data can be observed up to channel 25. The correction of the observed count rate for small source extraction cell size is therefore difficult. To ensure that all the soft counts were accumulated for each spectrum and light curve, source regions were defined as circles of radii $200''$ centered on the target where possible. Exclusion regions also had to be set to mask out the contaminating counts from the nearby serendipitous sources (Fig. 1). In some cases this meant that a small correction for lost counts had to be made (using the formulae in Hasinger et al. 1992). Background regions were selected from source-free areas within the inner region of the PSPC (with off-axis angles $< 20'$).

3.1.2. Excess Companions

Surprisingly, all of the observations presented here showed serendipitous X-ray sources unusually close to the Seyfert 2 targets in every field.

Figures 1a–1g show the PSPC images of each of the Seyfert 2 fields. The scaling is not the same for each panel but was optimized for display purposes. The direction of wobble of the spacecraft is illustrated by the double-headed arrow in each case. It is immediately obvious that the close serendipitous

TABLE 1
ROSAT SEYFERT 2 OBSERVING LOG

Source	z^a	R.A. ^a	Decl. ^a	Observation Time (s)	Date	SASS Version
Mrk 573	0.0172	01 ^h 43 ^m 57 ^s .7	+02°20'59"	12935	1992 Jan 29–30	5_6
Mrk 372	0.0310	02 49 20.6	+19 18 15	12678	1992 Aug 15–22	5_8
NGC 1365	0.0055	03 33 36.5	−36 08 17	2577	1992 Aug 22–23	5_8
				6214	1993 Feb 5–10	6_2
Mrk 3	0.0136	06 15 36.3	+71 02 15	4786	1991 Mar 13–28	5_3_2
				8433	1992 Mar 13–Apr 6	5_7
Mrk 78	0.0371	07 42 41.7	+65 10 37	14057	1991 Mar 15–19	5_3_2
Mrk 273	0.0373	13 44 42.0	+55 53 12	17396	1992 Jun 19–22	5_8

^a Optical positions in J2000. Positions and redshifts from Véron, Cetty, & Véron 1989.

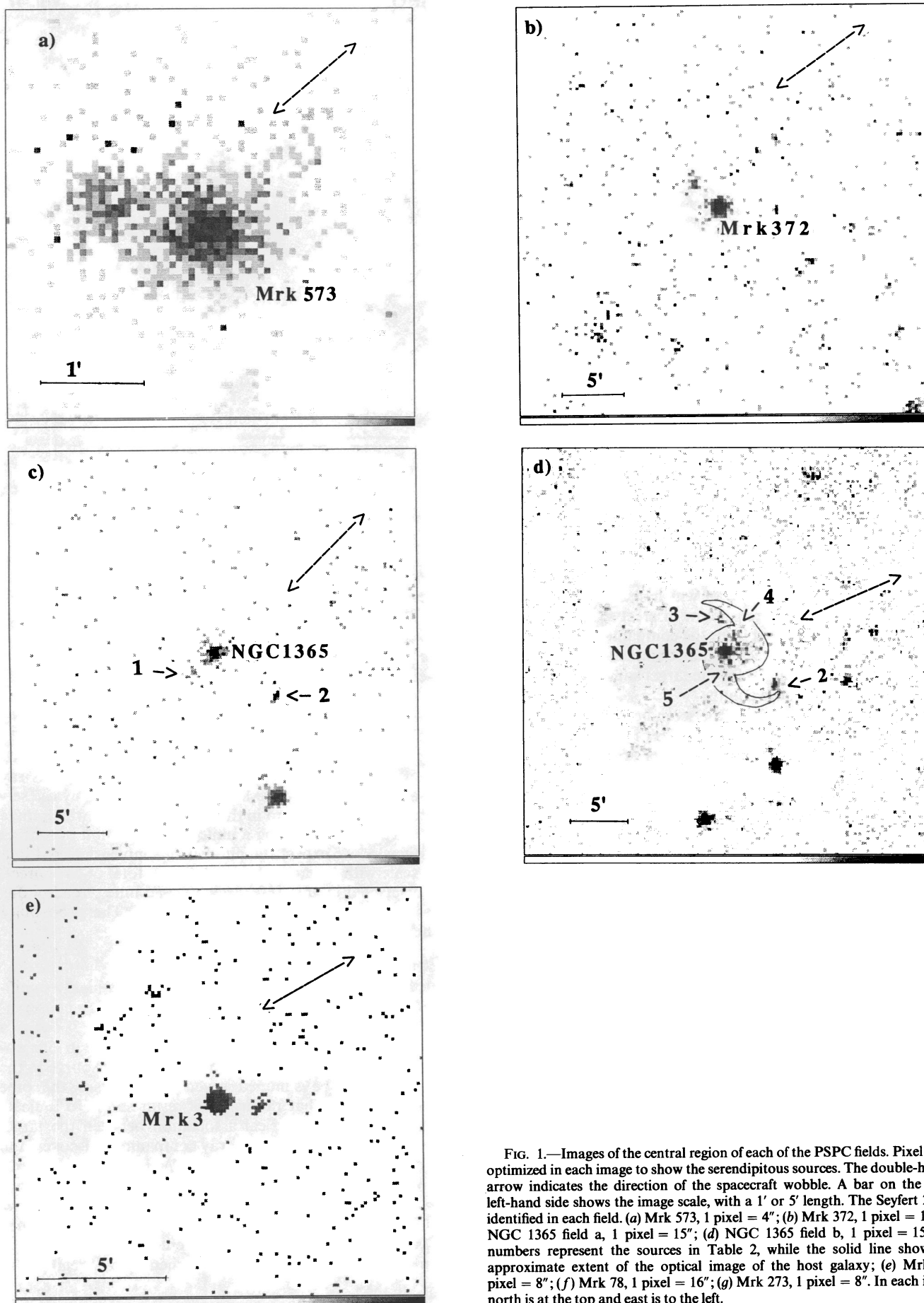


FIG. 1.—Images of the central region of each of the PSpC fields. Pixel size is optimized in each image to show the serendipitous sources. The double-headed arrow indicates the direction of the spacecraft wobble. A bar on the lower left-hand side shows the image scale, with a 1' or 5' length. The Seyfert 2's are identified in each field. (a) Mrk 573, 1 pixel = 4"; (b) Mrk 372, 1 pixel = 16"; (c) NGC 1365 field a, 1 pixel = 15"; (d) NGC 1365 field b, 1 pixel = 15"; the numbers represent the sources in Table 2, while the solid line shows the approximate extent of the optical image of the host galaxy; (e) Mrk 3, 1 pixel = 8"; (f) Mrk 78, 1 pixel = 16"; (g) Mrk 273, 1 pixel = 8". In each image, north is at the top and east is to the left.

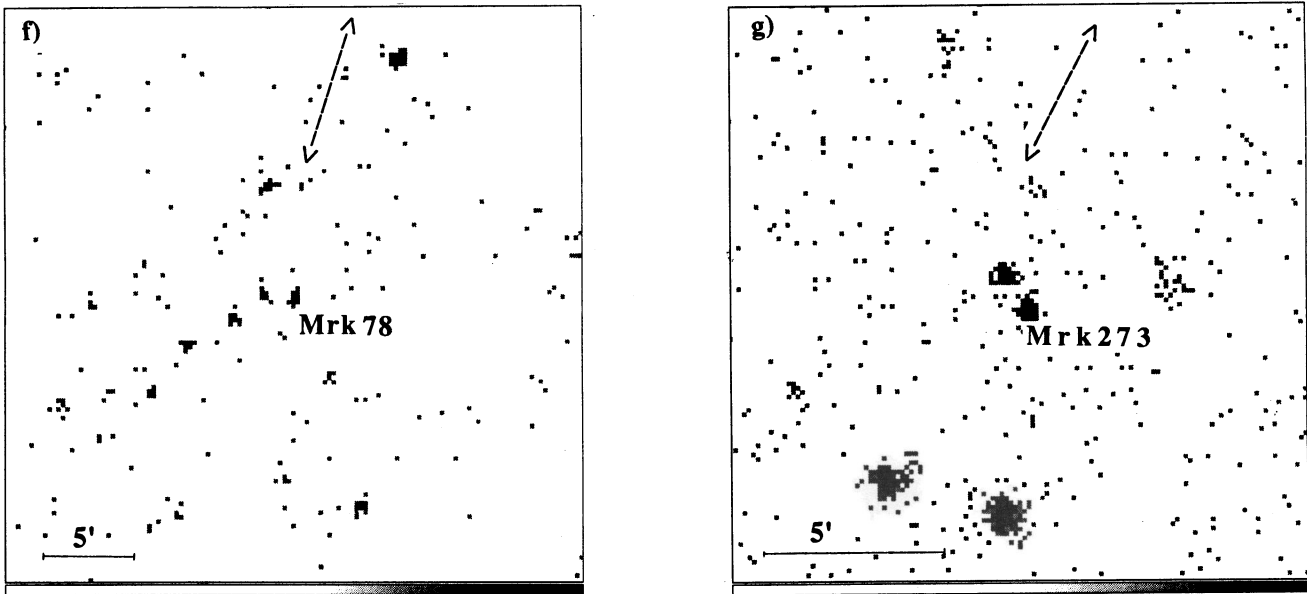


FIG. 1—Continued

sources cannot be due to errors in the aspect reconstruction. We also checked each observation interval individually and confirmed that these sources were not due to overlaying slightly offset images on top of each other. The observation of other bright sources in each field, none of which showed any close companions, confirms these are genuine discreet sources. Sufficient counts were accumulated from the companion sources to Mrk 573 and Mrk 273, for spectra to be obtained. The spectra were different to those obtained for the target sources, confirming the discrete origin of those counts.

Table 2 gives the count rates of the serendipitous sources. It is important to note here that in some cases (notably Mrk 573, Mrk 273, and Mrk 78) the nearby sources are a significant fraction of the count rates of the Seyfert 2 target; thus all previous X-ray observations of these Seyfert 2's will be significantly contaminated, as these sources have never been spatially resolved before in the X-ray regime, even by the IPC. This means that the flux variability claimed for Mrk 78 (Urry et al. 1986) may have been attributable to one of the other unresolved sources. The target sources themselves were all fairly weak, and a comparison of the radial profiles of these sources and the point-spread function of the PSPC detector showed no evidence for extended emission (masking out the nearby serendipitous sources). NGC 1365 showed evidence for extended emission in the *Einstein* observation. In this PSPC observation, the image shows five distinct X-ray sources within the host galaxy or coincidentally aligned with it. The unresolved emission from these sources can easily explain the detection of extended emission in the *Einstein* observation.

To determine whether the observation of the serendipitous sources in Table 2 is by chance alignment, or whether those sources are likely to be physically associated with the Seyfert 2 targets, we have counted the total number of sources detected within the inner region (i.e., within a radius of 20') of the PSPC for the seven fields. To do this we ran the COSMOS detection algorithm and determined the number of sources $> 3\sigma$ above the background in the 0.1–2.0 keV band. A vignetting and exposure correction was folded to each detected source, we note that we used only the central region of the PSPC in each

field, to minimize problems in correcting for the loss of sensitivity as one moves outward toward the edge of the detector (due to vignetting and reduced exposure). The flux limit used was 3×10^{-14} ergs cm^{-2} s^{-1} , the flux of the dimmest source significantly detected in this sample of fields in the 0.1–2.0 keV band (Table 2). The NGC 1365 data came in two separately processed intervals, as listed as such in Table 2, and were thus for the spatial analysis were treated as two observations (as opposed to Mrk 3, where the data were taken in two widely separated intervals, but processed into one dataset). Summing the seven fields, a total of 55 sources were detected above the stated flux limit, in the annulus from 3' to 20' radius, while 16 sources were detected in the inner 3' radius circle. As the pointing positions were a priori selected to place a known X-ray source at the field center, we henceforth consider only the serendipitous sources detected in the central 3' cell, of which there are nine (Table 2). Assuming a uniform distribution of sources across the sky, we expect the number of sources detected in a cell, to scale with the area of the cell. For a total of 64 sources, 55 were detected in area 8600 arcmin², and nine serendipitous sources were detected in area 198 arcmin². The probability that this is by chance is then

$$\text{Prob} = 64!/(9! 55!) \times 0.023^9 \times 0.9770^{55} \sim 1.4 \times 10^{-5},$$

indicating that the clustering of X-ray sources is highly significant. (The exclusion of the target sources made this a conservative calculation.) The source density in the inner 3' cell is a factor of 8 higher than the mean source density in our co-added field! We would expect one serendipitous source in the inner 3' cell of the summed seven fields versus the nine observed in within that radius. This result seems to indicate that there may be a physical association between the target sources and the serendipitous X-ray companions discovered in these data. Using the published $\log N$ – $\log S$ (Branduardi-Raymont et al. 1993) we expect 126 sources per square degree down to a flux limit of 1×10^{-14} ergs cm^{-2} s^{-1} ; thus we would expect two serendipitous sources in the seven summed fields within a 3' cell. As the fields were not all long enough exposures to attain this flux limit, then two serendipitous

TABLE 2A
SERENDIPITOUS SOURCES CLOSE TO THE CENTER OF THE FIELD OF VIEW

SOURCE	COORDINATES ^a	COUNTS ^b	COUNTS PER SECOND	SEPARATION ^c	
				Arcminutes	Kiloparsecs
Mrk 573	1 ^h 43 ^m 57 ^s .7, +02°20'53"	826	0.064		
Companion	1 44 1.5, +02 21 06	268	0.021	0.41	11
Mrk 372	2 49 20.6, +19 18 23	3450	0.272		
Companion	2 49 28.5, +19 20 12	58	0.005	2.83	139
NGC 1365a	3 33 36.6, -36 08 02	298	0.115		
Companion 1	3 33 44, -36 09 32	28	0.011	1.76	15
Companion 2	3 33 13, -36 11 39	18	0.007	3.72	32
NGC 1365b	3 33 35.8, -36 08 22	891	0.143		
Companion 1		<9	<0.001	1.76	15
Companion 2	3 33 12.0, -36 11 43	92	0.015	3.72	32
Companion 3	3 33 39.8, -36 05 10	20	0.003	3.25	28
Companion 4	3 33 31.9, -36 06 46	18	0.003	2.06	18
Companion 5	3 33 34.2, -36 09 29	18	0.003	2.75	23
Mrk 3	6 15 35.6, +71 02 11	963	0.073		
Companion	6 15 14.5, +71 01 58	42	0.003	1.83	39
Mrk 78	7 42 41.0, +65 10 39	174	0.012		
Companion 1	7 42 58.9, +65 11 03	34	0.003	2.42	142
Companion 2	7 43 14.7, +65 09 36	73	0.005	2.21	130
Mrk 273	13 44 40.4, +55 52 59	368	0.021		
Companion	13 44 46.3, +55 53 58	194	0.011	1.94	114

^a Coordinates are the X-ray positions in J2000.

^b Source counts in PI channels 12–200 inclusive.

^c Assuming the serendipitous source is at the same redshift as the Seyfert galaxy.

TABLE 2B
BORESIGHT-CORRECTED POSITIONS FOR THE
SERENDIPITOUS SOURCES IN J2000

Source	Position
Mrk 573:	
Companion	1 ^h 44 ^m 1 ^s .5, +02°21'12"
Mrk 372 field:	
Companion	2 49 28.5, +19 20 04
NGC 1365 field:	
Companion 1	3 33 44, -36 09 47
Companion 2 ^a	3 33 12.9, -36 11 47
Companion 3	3 33 40.5, -36 05 5
Companion 4	3 33 32.6, -36 06 41
Companion 5	3 33 34.9, -36 09 24
Mrk 3 field:	
Companion	6 15 15.2, +71 02 02
Mrk 78 field:	
Companion 1	7 42 59.6, +65 11 1
Companion 2	7 43 15.4, +65 09 34
Mrk 273 field:	
Companion	13 44 47.9, +55 54 11

^a Mean position from the two observations of this field.

sources is an overestimate, yet it falls far short of the nine detected sources.

Unfortunately we cannot make a useful comparison with the PSPC Seyfert 1 observations, partly because the exposure times on those bright AGNs were typically only a few thousand seconds, and partly because the target sources were so bright, that nearby faint companion sources would be much harder to detect. In two Seyfert 1 fields for which we had an

exposure time comparable to the observations presented here, no companion sources were detected within a 3' cell around the target source.

3.1.3. Possible Identifications of the Serendipitous Sources

None of the X-ray companion sources listed in Table 2 have optical identifications in the literature. An optical follow-up program is necessary to confirm whether these close X-ray sources are actually associated with the Seyfert 2's, or whether they are just foreground or background sources along the line of sight. We are able to make some statements about the optical identifications of these sources, however, based on approximate optical magnitudes from archival plate data. The optical magnitudes, X-ray-to-optical flux ratios, and intrinsic X-ray luminosities of the companions put useful constraints on the likely optical identifications. The separation of the companion source from the AGN also offers some clues. In the case of nearby galaxies such as NGC 1365 it seems likely we are resolving bright X-ray sources within the host galaxy, while in the case of the distant Mrk 78, the sources are more likely to be low luminosity AGNs associated with Mrk 78 or background AGNs.

When comparing the optical and X-ray positions of the sources, one should keep in mind the uncertainties involved in the determination of the X-ray positions. Boresight errors can affect the absolute position determination. Previously, systematic discrepancies have been noted between the optical and X-ray positions of *ROSAT* targets. In an MPE study the 1σ scatter of the distribution of optical versus X-ray positions was 6".1 for the PSPC (B) and 6".4 for the HRI. The PSPC data showed a systematic offset of 6".9, while the HRI showed negligible systematic offset (the HRI always had a boresight correction of 10" in the Y-direction). For a long time, no correction was made to SASS to account for this systematic effect in the

PSPC data. This was because there was a large scatter in the offsets noted (up to $20''$), and the effect was not understood. Finally, though, it was decided to correct the SASS for the mean offset of $6''$ in the PSPC data. The correction was implemented in 1992 December at MPE (SASS 6_2), and affects data processed since then (or since 1993 January in the USA), which are data taken since approximately 1992 September. Also, all reprocessed ("Rev1") data will have this (or an updated) boresight correction folded in. There were some inaccuracies in the original study however, notably that the nearest SIMBAD source was always taken as the optical counterpart, when in fact that was not always the ID with the best position. This meant of course that the boresight error was originally underestimated. A new study then showed the deviations from expected (SIMBAD) positions still lay clustered around $3''$ – $4''$ on the positive detector y -axis. Another $3''$ – $4''$ correction is required, in the same sense as the original correction.

These boresight corrections do not get rid of the scatter in the difference between optical and X-ray positions. It is thought that this may be due to star tracker problems. It seems that the star tracker has some variations in quantum efficiency between the pixels. This means that the centroiding to get the position of the guide stars can be skewed. It seems unlikely that this can be corrected for, as not all of the star tracker pixels are calibrated. This seems like the most likely origin of the large scatter in the discrepancies in X-ray positions mentioned above (Kuerster & Hasinger 1992).

Relative position determination is accurate to $5''$ – $10''$, depending on the number of detected photons. Comparison of the optical positions of the target sources in Table 1 with the X-ray positions determined from the PSPC data in Table 2, show some discrepancies between the optical and X-ray positions, due to a combination of these errors. The largest discrepancy is $\sim 16''$ for Mrk 273. To minimize the error in position of the serendipitous sources, we corrected the X-ray positions of the serendipitous sources by the boresight error estimated for each field. We list the X-ray positions derived from the PSPC data for the target sources and companions in Table 2A. We estimate the boresight correction for the field from the difference between the optical and X-ray position for the Seyfert 2 target in each case. We then make a correction to the companion position based on that comparison, and list the corrected positions of the companion sources in Table 2B. We then use those corrected positions to try and make the source identification.

The ratio $\log(f_x/f_{\text{opt}})$, where f_x is flux density at 1 keV and f_{opt} is flux density in the V band, proved to be a useful discriminant among different categories of identification for the *Einstein* Medium Sensitivity Survey (EMSS; Gioia et al. 1990). X-ray-selected BL Lac objects have very high values of this ratio, as do supernova remnants, followed by clusters of galaxies, AGNs, galaxies, late-type stars, and early-type stars, in that order (see Stocke et al. 1991). Since AGNs and BL Lac objects can vary in both X-ray and optical flux, and the archival optical plates discussed below were taken at very different times from the X-ray observations, application of these guidelines to our derived values will work only very roughly for AGNs and BL Lac objects. A factor of 2 variation is quite possible, but a factor of 10 is unlikely, so the ranges given by Stocke et al. (1991) should be extended by something between 0.5 and 1 in both directions for AGNs and BL Lac objects. Also, the magnitudes estimated from the archival plate material are highly uncertain, by perhaps ± 0.5 , particularly for the fainter objects, and this can affect $\log f_x/f_{\text{opt}}$ by ± 0.2 or so.

All searches for optical counterparts were made using digitized optical plates available in the GASP system at the Space Telescope Science Institute. Notes on the individual fields follow.

Mrk 573.—There is a candidate identification for the companion within $\sim 3''$ of the corrected X-ray position (Table 2B). This object is brighter in the blue IIIa-J (B) plate than the red POSS-E plate, ($B \sim 19.4$ in 1983 compared to $R \sim 20.1$ in 1952). It is approximately pointlike and the optical plate positions are

$$1^{\text{h}}44^{\text{m}}1^{\text{s}}.97, +2^{\circ}21'14''.83 \quad [\text{IIIa-J (B) 1982.9}]$$

$$1^{\text{h}}44^{\text{m}}2^{\text{s}}.17, +2^{\circ}21'13''.66 \quad (\text{POSS-E 1951.7}) .$$

The ratio of X-ray to optical flux is $\log f_x/f_{\text{opt}} = 0.3$ (with large errors), commensurate with an AGN, BL Lac object, or supernova remnant, but unlike stars or most galaxies. This object is $\sim 1'$ east of Mrk 573, or ~ 11 kpc projected distance at the redshift of Mrk 573. There is no obvious connection between this and the small-scale extended optical emission noted in Wagner & Anton (1989).

Another possible optical counterpart lies at $01^{\text{h}}44^{\text{m}}0^{\text{s}}.6, +2^{\circ}21'00''$ (POSS-E 1951.7). This is slightly brighter on the red plate but barely detected on the blue plate. This second source would have $\log f_x/f_{\text{opt}} > 0.3$, and if it is the correct identification it is unlikely to be an AGN.

The X-ray spectrum of the serendipitous source was $\Gamma = 1.9$ ($+0.8, -0.7$) and column $N_{\text{H}} = 7.6 \times 10^{19}$ ($< 3.2 \times 10^{20}$ cm^{-2}) with 0.1–2.0 keV flux of 6.4×10^{-14} $\text{ergs cm}^{-2} \text{s}^{-1}$. At the distance of Mrk 573, the X-ray luminosity of the companion would be $\sim 5.0 \times 10^{41}$ ergs s^{-1} , like a very low luminosity AGN or an elliptical galaxy. If the source were a galaxy or AGN at the same distance as Mrk 573, however, we would be able to resolve the galaxy optically. The optical candidates are point sources; thus if the correct identification is an AGN, it must be a background source.

Mrk 372.—Quick-V and POSS-E plates were available. There is a pointlike object at

$$2^{\text{h}}49^{\text{m}}29^{\text{s}}.30, +19^{\circ}20'8''.27 \quad (\text{Quick-V 1983.0})$$

$$2^{\text{h}}49^{\text{m}}29^{\text{s}}.40, +19^{\circ}20'8''.16 \quad (\text{POSS-E 1951.9}) .$$

The object is reddish ($V \sim 17.8, R \sim 17.4$) and $\log f_x/f_{\text{opt}} \sim -1.6$, like a galaxy or late-type star. At the distance of Mrk 372, the 0.1–2.0 keV X-ray luminosity is 2.2×10^{41} ergs s^{-1} , plausible for a galaxy or low-luminosity AGN. Again, the pointlike nature of the optical source suggests the late-type star may be the more appropriate identification.

NGC 1365.—Our *ROSAT* PSPC observations show five X-ray sources coincident with the galaxy NGC 1365; these total $\sim 16\%$ of the soft X-ray count rate of NGC 1365. In the first observation of this field (a), there are two companions; the X-ray positions for both may be uncertain as discussed above, because there are only a few photons detected for each. In the second and longer observation (b), we detect four sources close to NGC 1365. In the second observation, companion 1 was not detected, and the upper limit on count rate was a factor of 10 lower than the flux in the first observation (Table 2A); three new sources were detected, however (which would not have met the significant detection criteria in the first, shorter, observation).

Figure 1d shows the contour representing the extent of the optical image of NGC 1365, overlaid on the second PSPC observation. It is immediately obvious that (assuming the

sources lie at the same distance as NGC 1365) all five of the serendipitous sources lie within the host galaxy or spiral arms, the detected X-ray sources extend out along the spiral arms, and the two farthest sources from the nucleus appear to lie at the tips of the spiral arms (companions 2 and 3). Given the coincidence of the X-ray companion sources with the host galaxy and spiral arms, we consider it more likely that these serendipitous sources are associated with the Seyfert 2 galaxy than that they are background AGN.

NGC 1365 was previously observed twice by *Einstein* and detected with the IPC but not the MPC (Maccacaro, Perola, & Elvis 1982). Those IPC observations were suggestive of extended emission in this source, with the extended region estimated to be $\sim 40''$ in extent. In addition the *Einstein* IPC image showed two weak but distinct sources close to NGC 1365. Fabbiano, Kim, & Trinchieri (1992; see their Fig. 7) show an IPC image of this field and X-ray sources consistent with the positions of companions 2 and 3 (Table 2) are evident in their data.

Only IIIa-J plates are available (blue) for optical identifications. There is no optical counterpart at the X-ray position of the first companion. It lies along the outer edge of the southern spiral arm. The optical plate was taken in late 1976, however, and this source is obviously variable at least in the X-ray regime, as it was not detected in the second observation (6 months after the first). At the distance of NGC 1365, the X-ray luminosity in the first observation is $\sim 1.2 \times 10^{40}$ ergs s^{-1} . For the plate limit the ratio of X-ray-to-optical flux is $\log f_x/f_{opt} > 0.5$, implying a rather high-luminosity X-ray binary in NGC 1365 as the X-ray source. Serendipitous sources of a similar luminosity were noted in *Einstein* observations of NGC 5548 and NGC 1566 (Fabbiano et al. 1992). The apparent fading of the X-ray source between the two observations leaves a supernova as a possible identification, although we cannot rule out an X-ray binary system.

For the second companion, five objects are visible, all plausible candidates for the X-ray source (although b is the closest to the position in Table 2B). Their properties are summarized in Table 3.

The plate limit of 20.5 gives a ratio $\log f_x/f_{opt} > -0.5$ if the correct optical counterpart is blank sky, at the distance of NGC 1365, the X-ray luminosity is $\sim 8 \times 10^{39}$ ergs s^{-1} , consistent with a Galactic binary source. The X-ray flux increased by a factor of 2 between the first and second observations (and the source was detected in the *Einstein* IPC image, although no flux was quoted; Fabbiano et al. 1992). This variability rules out a supernova or supernova remnant as the identification of companion 2.

Osmer, Smith, & Weedman (1974) have shown that there are many bright H II regions around the nucleus of NGC 1365; this work was continued in Alloin et al. (1981) who give positions of the hot spots in NGC 1365. The fourth companion is

within $8''$ of the H II region L15 reported by Alloin et al. (1981) and lies on the northern spiral arm of NGC 1365. The numerous H II regions discovered in NGC 1365 imply a very low abundance gradient in NGC 1365.

The third and fifth companions lie embedded within the host galaxy, and thus it was not possible to make an identification based on POSS plate data.

Mrk 3.—If the companion is at the distance of Mrk 3, its X-ray luminosity is only $\sim 2 \times 10^{40}$ ergs s^{-1} , too low for an AGN, BL Lac object, or cluster of galaxies. Nothing is visible on the Quick-V; on the POSS-E (red) plate, there is a possible candidate west of X-ray position, near the plate limit ($V \sim 20.1$) at

$$6^h 15^m 11^s 24, +71^\circ 1' 58'' 21 \quad (\text{POSS-E 1954.1}).$$

The information from the X-ray-to-optical flux ratio, $\log f_x/f_{opt} \sim -0.8$, is not helpful: the companion could be a star, galaxy, or an AGN. If the correct identification is the blank field, then $\log f_x/f_{opt}$ goes up and could be commensurate with an AGN, cluster of galaxies, or BL Lac object. Given the X-ray flux of the companion, if the correct identification is an AGN, BL Lac object, or cluster of galaxies, it must be a chance superposition of a background source.

Although an extended emission component is noted in radio and optical observations of this source (Wagner & Anton 1989), this extends in the opposite direction to the companion source and on a much smaller scale.

Mrk 78.—Two plates were available: Quick-V and POSS-E. Near the position of the first companion, the only thing visible on Quick-V or POSS-E is a bright, red object ($V \sim 16$, $R \sim 14$) about $25''$ northeast. The X-ray flux and position come from 34 photons so it is just plausible that this is the correct optical counterpart. In this case $\log f_x/f_{opt} \sim -2.5$, possibly a star. The alternative identification is a blank field, yielding $\log f_x/f_{opt} > -1.2$; this could still be a star, but is now within the range for a galaxy, cluster of galaxies, AGN, or even a BL Lac object. At the distance of Mrk 78, the X-ray luminosity of this companion is $\sim 1.6 \times 10^{41}$ ergs s^{-1} , so any extragalactic identification except for a galaxy, Seyfert 2, or supernova would have to be more distant than Mrk 78. The optical source is not significantly extended in the plates, and so the star may be the best guess identification in this case.

For the second companion, there are two pointlike optical candidates separated by $< \sim 5''$, both located close to the companion position. Optical positions are

$$7^h 43^m 14^s 17, +65^\circ 9' 29'' 8 \quad (\text{Quick-V 1983.2})$$

$$7^h 43^m 14^s 20, +65^\circ 9' 26'' 26 \quad (\text{Quick-V 1983.2})$$

$$7^h 43^m 14^s 30, +65^\circ 9' 31'' 33 \quad (\text{POSS-E 1955.3})$$

$$7^h 43^m 14^s 40, +65^\circ 9' 25'' 25 \quad (\text{POSS-E 1955.3}).$$

TABLE 3
PROPERTIES OF CANDIDATES FOR SECOND COMPANION TO NGC 1365

Candidate	Optical Position (1976.9)	Approximate B Magnitude	$\log f_x/f_{opt}$	Comments
a.....	3 ^h 33 ^m 14 ^s 31, $-36^\circ 12' 14''.48$	18.0	-1.5	Galaxy, star (fuzzy?)
b.....	3 33 12.86, $-36 11 54.29$	18.7	-1.3	AGN?, galaxy, star
c.....	3 33 12.02, $-36 11 49.32$	18.1	-1.5	Galaxy, star
d.....	3 33 11.29, $-36 11 39.71$	20.0	-0.7	AGN, cluster, galaxy
e.....	3 33 12.50, $-36 11 09.97$	15.8	-2.4	Mid-early star?(fuzzy?)

Comparison of the Quick-V and POSS-E plates implies the southern object is bluer than the northern object. We do not have separate optical magnitude estimates at this point, as the automatic routine extracts a summed flux for these two objects. Assuming they have equal magnitudes, the X-ray-to-optical flux ratio (for each) is $\log f_x/f_{\text{opt}} \sim -2$, indicative of stars. At the (unlikely) distance of Mrk 78, the X-ray luminosity would be $\sim 3 \times 10^{41}$ ergs s^{-1} .

Mrk 273.—There is one X-ray companion with two possible optical counterparts:

$13^{\text{h}}44^{\text{m}}47^{\text{s}}.84$, $+55^{\circ}54'37''.06$ (1983.2 V, faint object)

$13^{\text{h}}44^{\text{m}}44^{\text{s}}.30$, $+55^{\circ}54'28''.23$ (1983.2 V, bright object)

$13^{\text{h}}44^{\text{m}}48^{\text{s}}.19$, $+55^{\circ}54'35''.14$ (1955.3 POSS-E, faint object)

$13^{\text{h}}44^{\text{m}}44^{\text{s}}.54$, $+55^{\circ}54'26''.67$ (1955.3 POSS-E, bright object)

The brighter candidate is $\sim 42''$ east (and a bit north) of the nominal position and so is unlikely to be the correct identification. If this is the correct identification, then $V \sim 10.3$, $R \sim 10.4$, and $\log f_x/f_{\text{opt}} \sim -4.3$, clearly a star, and a chance superposition.

The fainter object is $\sim 15''$ NW of the nominal position; the optical plate suggests the source may be a bit extended. It has $V \sim 17.5$, $R \sim 17.6$, and $\log f_x/f_{\text{opt}} \sim -1.4$. This is in the likely

range for a galaxy (and just within the range for an AGN), which would have the right X-ray luminosity to be in the vicinity of Mrk 273. At the distance of Mrk 273, the X-ray luminosity is 6.3×10^{41} ergs s^{-1} ; thus the source could be a Seyfert 2 if associated with Mrk 273 but could be a more luminous AGN if it is a background source. The spectrum of the serendipitous source was $\Gamma = 1.9 (+0.9, -0.8)$ and $N_{\text{H}} \sim 3.9 (+5.9, -3.3) \times 10^{20}$ cm^{-2} , consistent with an AGN spectrum, with a 0.1–2.0 keV flux of 9.6×10^{-14} ergs cm^{-2} s^{-1} .

3.2. Timing Analysis

Light curves were constructed using the same regions as for the spectral analysis, in PI channels 12–200 (inclusive). The background-subtracted light curves are shown in Figure 2, with the relatively large data gaps removed for illustrative purposes. The dotted vertical lines separate the individual data “good time intervals” (GTIs). Each background-subtracted light curve was tested for variability (Table 4); the source and background light curves do not necessarily have the same number of time bins (background light curves were rebinned such that enough counts were accumulated per bin for χ^2 statistics to be applied).

The only sources to exhibit significant variability (Table 4) were Mrk 372 and NGC 1365. The flux of Mrk 372 changed by approximately a factor of 2.2 on a timescale of 12,000 s (the

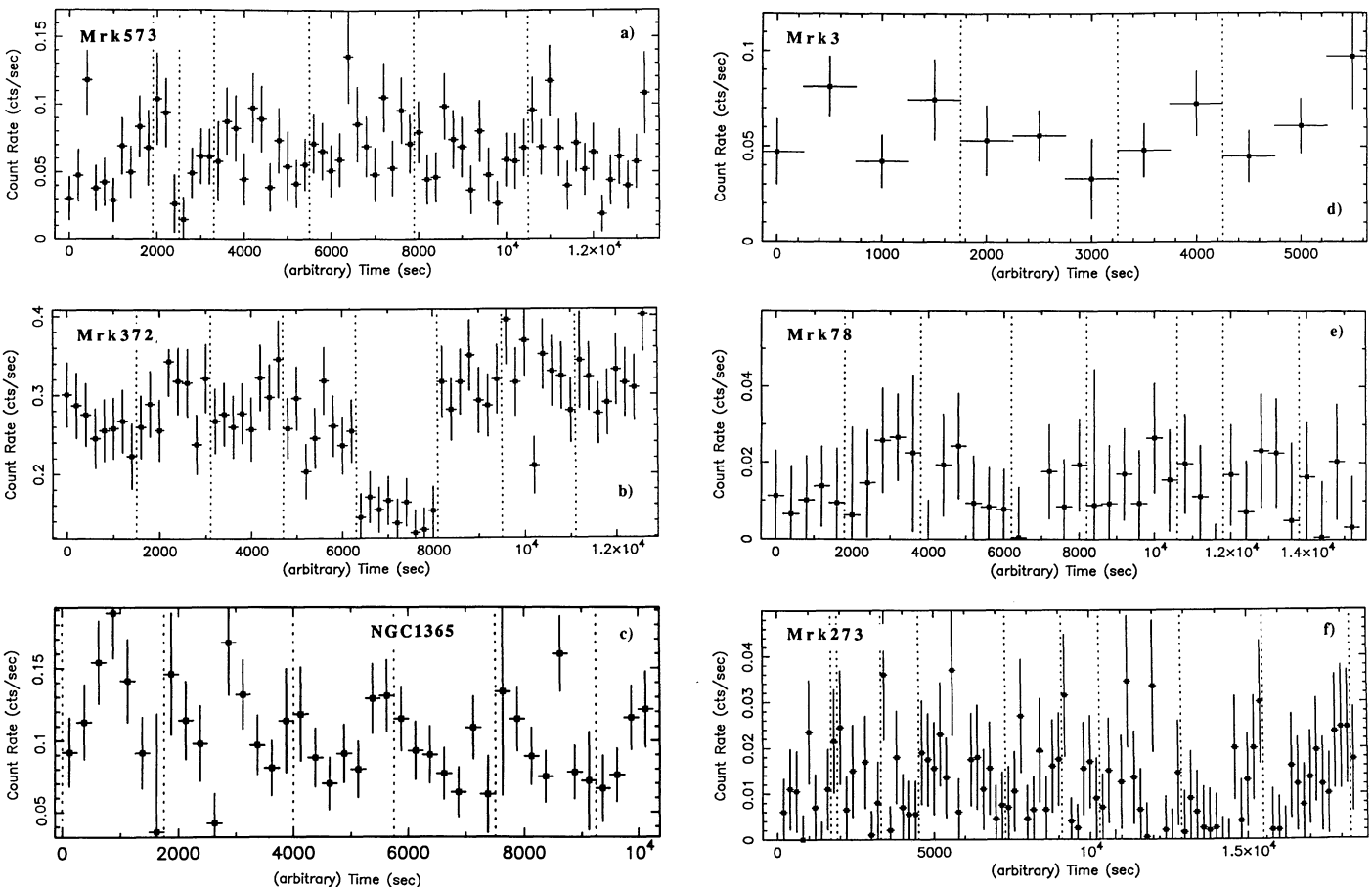


FIG. 2.—The background-subtracted light curves of (a) Mrk 573, 200 s bins; (b) Mrk 372, 200 s bins; (c) NGC 1365 (a + b), 250 s bins; (d) Mrk 3, 500 s bins; (e) Mrk 78, 400 s bins; (f) Mrk 273, 200 s bins. The gaps in the light curve due to earth occultation, SAA passages, and the scheduling pattern of *ROSAT* have been removed, for illustrative purposes. The dotted vertical lines distinguish the individual GTIs.

TABLE 4
TIMING ANALYSIS

Source	χ_r^2 Source ^a	P ^b	χ_r^2 Background
Mrk 573	73/67	20%	82/67
Mrk 372	102/60	0.1	56/49
NGC 1365	61/41	5	46/41
Mrk 3	10/12	60	27/18
Mrk 78	22/39	99	65/35
Mrk 273	73/93	95	457/104

NOTE.—All light curves were extracted in the 0.1–2.0 keV band and are shown in Fig. 2. The light curves were binned to a minimum of ~ 15 counts per bin, so that a χ^2 test could be applied.

^a Background-subtracted.

^b Probability of exceeding χ_r^2 (Source) by chance.

12,000 s gap between the good time intervals has been removed in Fig. 2b); the flux of NGC 1365 also shows factor of 2 variations but at a much lower level of significance (Fig. 2c). The Mrk 372 variability is reminiscent of Seyfert 1 continuum variability (discussed further in § 4). The NGC 1365 light curve, however, is contaminated by the serendipitous sources noted in Table 2 and thus may reflect the variability of those sources rather than the active nucleus.

The variability timescales are sufficiently long, and the amplitude of the effect is sufficiently large that the variability cannot be due to the periodic occultation of the source by the PSPC coarse wire grid. All of the sources presented here were observed close to the center of the PSPC field of view, and thus none of the target sources suffered occultation by the PSPC support ribs. No evidence was found for significant hardness ratio variations as the source flux varied.

3.3. The Spectral Analysis

PSPC photon events are corrected for analog-to-digital converter nonlinearity, gain saturation effects, temporal and spatial gain variations, and window and electronic positional variations. The lower level discriminator for valid events is different for each observation (depending on the exact detector status; Hasinger & Snowden 1990). Consequently PI channels < 12 were excluded from the subsequent spectral data analysis (except for the first observation of Mrk 3, which was taken at a different gain state, for that observation, channels 9–200 were acceptable). At high energies, the PSPC response matrix is not currently valid above channel 250, and, as the mirror effective area falls off rapidly to high energies (and high-energy effective

area calibrations are currently under revision; G. Hasinger, private communication), we excluded PI channels 200 and above. The remaining PI channels were rebinned such that we obtained at least 20 counts in each bin, enabling χ^2 fitting techniques to be applied. The data were then compared to various trial spectral models.

The results of fitting a simple power-law model with low energy absorption are given in Table 5. The most recent official matrix, released from MPE in 1993 January, was employed. All parameters were allowed to be free. Errors are quoted at 90% confidence throughout (assuming one free parameter of interest; Lampton, Margon, & Bowyer, 1976), unless otherwise stated. The counts spectra, i.e., the data convolved with the detector response, are shown in Figures 3a–3f (upper panels), along with the best-fitting model. The lower panel in each case shows the corresponding data minus model residuals. The spectra were also systematically fitted with the absorption fixed at the Galactic line-of-sight value from Stark et al. (1993), which made many of the fits statistically unacceptable (Table 6).

Interestingly, the largest contributions to χ^2 are not at the lowest energies, but manifested as an excess of counts around 0.8 keV. For example, Figure 4 shows the counts spectrum and residuals for NGC 1365 and Mrk 3, when fitted with this constrained model. As the excess is indicative of the presence of line emission, a narrow (50 eV) Gaussian line component was added to the model. Those data for which the probability of exceeding χ^2 by chance was 5% or less (in Table 6) were refitted. The results are shown in Table 7. The only significant improvements were obtained for Mrk 3, NGC 1365, and Mrk 273. The addition of an emission line to the model is only a significant improvement to the fit when the absorption is fixed at the Galactic value. This is because, at low signal-to-noise ratio and with low energy resolution, one cannot distinguish between a line of high equivalent width, superposed on the continuum, and a much steeper and highly absorbed continuum form. One can see this by comparing the power-law indices and absorbing columns in Table 5 with the fit parameters in Tables 6 and 7.

Given the evidence for improvement to the fits with an emission-line component, we then systematically fitted the data with a power-law-plus-Raymond-and-Smith equilibrium plasma model, with fixed Galactic column. This model significantly improved the fit for four sources (Table 8), with a mean Raymond-Smith plasma temperature of ~ 0.46 keV. Interestingly, Mrk 372 was not suggestive of any line or thermal

TABLE 5
POWER-LAW MODEL: FREE PARAMETERS

Source	Γ	N_{H}^{a}	$N_{\text{H(gal)}}^{\text{a}}$	χ^2/bins	Flux ^b	Flux Ratio ^c	$L_{\text{soft}}^{\text{d}}$
Mrk 573	$3.50^{+0.39}_{-0.36}$	$4.46^{+1.15}_{-1.04}$	2.6	37.0/33	5.41	> 0.21	6.6
Mrk 372	2.17 ± 0.15	$8.55^{+1.10}_{-0.93}$	11.0	59.9/57	32.83		130
NGC 1365 (mean)	3.01 ± 0.27	$5.82^{+1.09}_{-1.02}$	2.0	78.4/40	9.90	> 0.35	1.1
Mrk 3 (mean)	$4.58^{+1.96}_{-1.07}$	$30.96^{+29.32}_{-13.90}$	8.7	41.0/32	6.33	0.013	4.8
Mrk 78	$2.70^{+3.98}_{-1.28}$	$7.01^{+5.75}_{-3.23}$	4.7	8.1/8	1.45	> 0.06	8.1
Mrk 273	3.01 ± 0.75	$5.53^{+3.80}_{-2.58}$	1.3	16.3/17	2.18	> 0.17	12.0

^a In units of 10^{20} cm^{-2} .

^b 0.1–2.0 keV band in units of $10^{-13} \text{ ergs cm}^{-2} \text{ s}^{-1}$.

^c Ratio of the 0.1–2.0/2–10 keV fluxes, where the 2–10 keV fluxes are observed fluxes or upper limits obtained by *Ginga*.

^d Observed 0.1–2.0 keV luminosity in units of $10^{41} \text{ ergs s}^{-1}$.

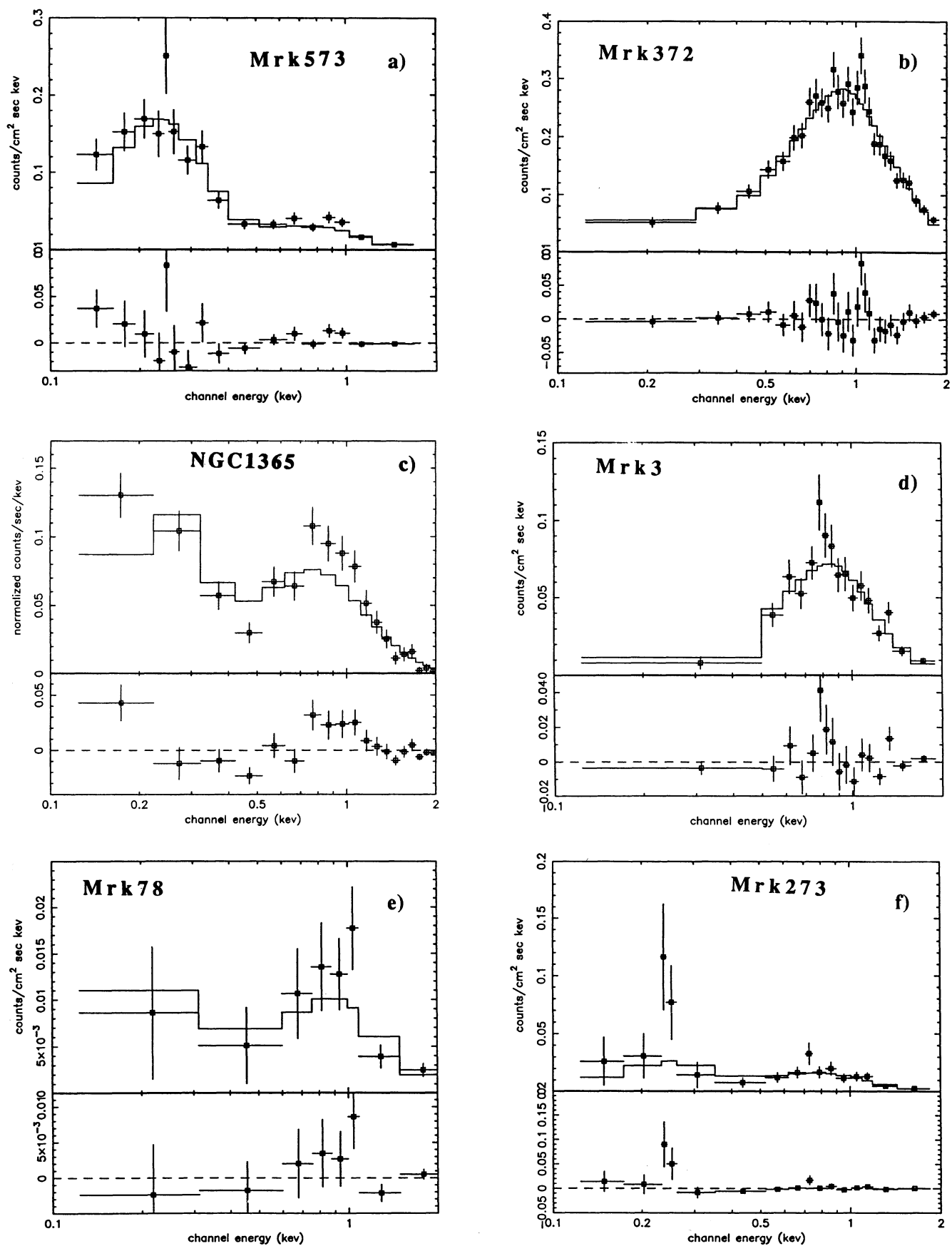


FIG. 3.—The counts spectra (*top*) and the data minus model residuals (*bottom*) after fitting an absorbed power-law model to the PI data for (a) Mrk 573, (b) Mrk 372, (c) NGC 1365 a, (d) NGC 1365 b, (e) Mrk 3, (f) Mrk 78, (g) Mrk 273. The solid line represents the best-fit model convolved with the detector response.

TABLE 6
SEYFERT 2 GALAXIES—POWER-LAW MODEL: FIXED NH

Source	Γ	χ^2/bins	χ_r^2/dof	$P(\chi^2)^a$	Flux ^b	L_{int}^c
Mrk 573	2.90 ± 0.10	45.3/33	1.46	$\sim 5\%$	4.7	5.7
Mrk 372	2.41 ± 0.10	67.4/57	1.31	~ 5	32.41	126
NGC 1365 (mean)	1.97 ± 0.09	121.0/40	3.03	< 0.1	7.78	1.0
Mrk 3 (mean)	2.65 ± 0.30	67.0/32	2.20	< 0.1	7.09	5.4
Mrk 78	2.27 ± 0.45	8.5/8	1.35	~ 20	1.29	7.5
Mrk 273	1.88 ± 0.19	24.8/17	1.65	~ 5	1.80	10.0

^a Probability of exceeding χ^2 by chance.

^b 0.1–2.0 keV band in units of 10^{-13} ergs cm^{-2} s^{-1} .

^c 0.1–2.0 keV band in units of 10^{41} ergs s^{-1} .

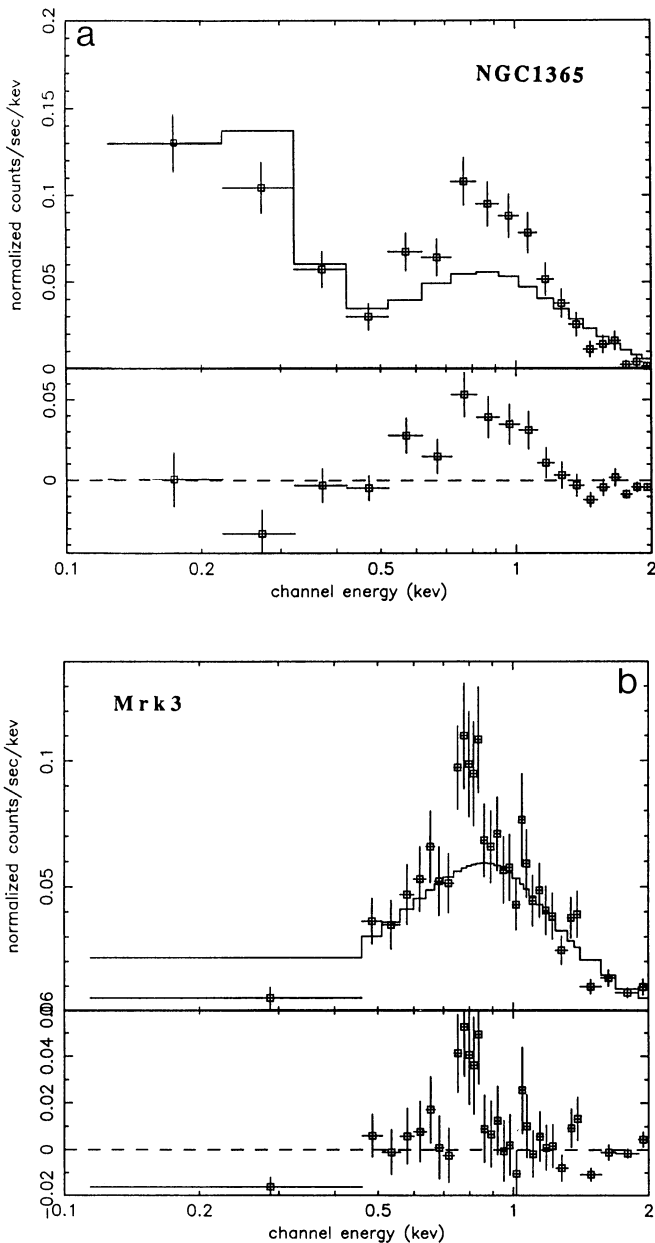


FIG. 4.—The counts spectra (top) and the data minus model residuals (bottom) after fitting an absorbed power-law model to (a) the NGC 1365 data and (b) the Mrk 3 (b field) data with the absorbing column fixed at the Galactic value in each case. The solid line represents the best-fit model convolved with the detector response.

component. We also note that the line equivalent widths in Table 7 are generally a factor of a few higher than those obtained for Seyfert 1 galaxies, in a similar analysis (Turner et al. 1993). The relatively strong soft emission line or blend in Seyfert 2 galaxies compared to Seyfert 1 galaxies suggests it arises either in or outside of the nuclear absorbing material.

The spectral indices in the simple model parameterization tend to be higher than those obtained for a similar sample of Seyfert 1 galaxies (although the mean index is not steeper at an interesting level of confidence). With the addition of an emission line to the model, the underlying photon index is flattened to become comparable to those obtained for a sample of Seyfert 1 galaxies (Turner et al. 1993). We note, however, that with these data it is not possible to unambiguously interpret the spectral complexity observed, as other models, such as complex absorbers, could produce similar residuals to those in Figure 4.

4. NOTES ON THE SPECTRA AND TIMING PROPERTIES OF INDIVIDUAL OBJECTS

4.1. Mrk 573

The nearby serendipitous source (discussed in § 3.1.3) was masked out when extracting a spectrum for Mrk 573. At the separation of $1'$, there should only be spectral contamination in the softest channels (< 25). An additional systematic error of 2% was folded into the affected channels to compensate for this.

4.2. Mrk 372

The X-ray spectrum of Mrk 372 is indistinguishable from that of a Seyfert 1 galaxy. The Seyfert 1 nature of the source (at least during this observation) is supported by the rapid X-ray variability observed (as noted in the previous section). The rapid variability suggests that the soft X-ray photons are observed directly (any scattering process would smooth out rapid variations) and that the active nucleus is relatively unobscured. A comparison between observed fluxes also shows the source to be a factor of ~ 5 ($\pm 10\%$) brighter during the *ROSAT* PSPC observation than it was when observed by the *Einstein* IPC (Kruiper et al. 1992), this variability is most likely attributable to Mrk 372, as the (previously unresolved) serendipitous source is a small fraction of the flux of Mrk 372 (Table 2). The unabsorbed soft X-ray luminosity of Mrk 372 (Table 4) is $\sim 1.3 \times 10^{43}$ ergs s^{-1} which is a factor of 10–100 greater than other sources in this sample. A sample of Seyfert 1 galaxies observed by *ROSAT* showed intrinsic 0.1–2.0 keV luminosities in the range $\sim (4 \times 10^{43})$ – (4×10^{44}) ergs cm^{-2} s^{-1} , and so Mrk 372 is at the low end of the range observed for Seyfert 1 galaxies (Turner et al. 1993).

TABLE 7
POWER-LAW PLUS EMISSION-LINE MODEL

Source	Γ	A^a	E_{line}	$A_{\text{line}}^{a,b}$	EW	χ^2/bins	F_{test}^c
Mrk 573	$3.09^{+0.20}_{-0.16}$	0.87 ± 0.08	0.85 ± 0.08	0.45 ± 0.26	314^{+180}_{-161}	34.1/33	<75%
Mrk 372	$2.43^{+0.10}_{-0.13}$	17.81 ± 2.00	0.70 ± 0.08	$0 < 20.0$	<200	67.4/57	0
NGC 1365 (mean)	2.12 ± 0.11	$2.55^{+0.40}_{-0.47}$	$0.81^{+0.04}_{-0.02}$	$1.93^{+0.42}_{-0.36}$	566^{+125}_{-105}	40.8/40	99.9
Mrk 3 (mean)	$2.26^{+0.55}_{-1.00}$	2.55 ± 0.60	0.78 ± 0.08	1.50 ± 0.95	333^{+137}_{-122}	41.7/32	99.5
Mrk 78 ^d
Mrk 273	$1.91^{+0.32}_{-0.36}$	0.43 ± 0.13	0.77 ± 0.10	0.39 ± 0.19	462^{+260}_{-229}	14/17	~95

NOTE.—Absorbing columns are fixed at the Galactic values, as listed in Table 4.

^a Normalization in units of 10^{-4} photons $\text{cm}^{-2} \text{s}^{-1} \text{keV}^{-1}$ defined at 1 keV for the continuum component.

^b Gaussian line widths frozen at 50 eV.

^c Significance of the improvement over the fit in Table 5, using the F -test.

^d Unable to converge on a unique solution, due to the low S/N in this dataset.

The derived *ROSAT* spectral index and column lie within the 1σ error range derived from the IPC data (Kruiper et al. 1992), and so no significant spectral variability is evident. At the epoch of the *ROSAT* observation, the X-ray source is unobscured (the column is consistent with the Galactic line-of-sight value).

The original optical observations reported Mrk 372 to be a type 2 Seyfert galaxy (Arakelian, Dibay, & Yesipov 1972). Gregory, Tift, & Cocke (1991) show that Mrk 372 has, in fact, a highly variable optical spectrum. In 1986 the spectrum was that of a Seyfert type 1.5 galaxy, with very broad permitted lines, and moderately broadened forbidden lines. In 1990 the spectrum was that of a Seyfert 1.9 galaxy; at $H\beta$ the broad-line component disappeared while observations near $H\alpha$ still showed a broad component. The fastest spectral variations observed to date showed a 65% change in $H\beta$ equivalent width between October and December of 1975 (Koski 1976). These changes observed in Mrk 372 are reminiscent of NGC 4151 emerging from its low state (Penston & Perez 1984). One possible explanation put forward for the change in the $H\alpha/H\beta$ ratio is that a dust cloud moved into the line of sight, preferentially absorbing the shorter wavelength photons. Variations in dust opacity could explain the optical variability. Changes in the dust content of the absorber may be driven by changes in the X-ray continuum (as the ionization parameter increases, the dust grains are destroyed).

4.3. NGC 1365

The mean spectrum of this source is not adequately fitted with a simple absorbed power-law model (Tables 4 and 5). Inspection of the residuals to such simple fits shows the greatest contribution to χ^2 to be in the excess of counts versus model around 0.8 keV (Figs. 3c and 4). The addition of an emission line or Raymond-Smith plasma component to the model improved the fit at 99.9% confidence. The spectrum has a significant contamination (but <16%) due to the nearby serendipitous sources (which unfortunately cannot be deconvolved from the nuclear spectrum). Given the large equivalent width of the emission-line complex, it seems most likely to be associated with the nuclear emission.

4.4. Mrk 3

A *Ginga* observation of Mrk 3 (Awaki et al. 1990) showed a flat spectrum source of $\Gamma = 1.3$ (photon) and a heavy absorption column $N_{\text{H}} \sim 5.9 \times 10^{23} \text{cm}^{-2}$, with an intrinsic 2–10 keV luminosity of $4 \times 10^{43} \text{ergs s}^{-1}$. A strong iron K line was detected (540^{+120}_{-50} eV). The line has a high equivalent width was because the continuum is heavily absorbed. Awaki et al. (1990) speculate that the nucleus of this Seyfert is heavily absorbed possibly by a torus, and that the soft X-rays observed by the *Einstein* IPC are X-rays scattered off this torus. Broad emission lines have been detected in the polarized flux spec-

TABLE 8
POWER-LAW + RAYMOND-SMITH MODEL: FIXED N_{H}

Source	Γ	A^a	kT (keV)	A_{Ray}^a	χ^2/bins	F_{test}^b
Mrk 573	$3.14^{+0.41}_{-0.22}$	$0.76^{+0.24}_{-0.34}$	$0.52^{+0.37}_{-0.27}$	$0.41^{+0.43}_{-0.19}$	30.9/33	99.9%
Mrk 372 ^c	$2.52^{+0.09}_{-0.11}$	$17.85^{+0.55}_{-0.55}$	0.46(f)	$0 < 0.35$	67.4/57	0
NGC 1365 (mean)	$2.22^{+0.22}_{-0.20}$	$1.74^{+0.64}_{-0.52}$	$0.55^{+0.14}_{-0.16}$	1.53 ± 0.76	35.5/38	99.9
Mrk 3 (mean)	$1.80^{+0.64}_{-0.24}$	$1.88^{+0.56}_{-0.72}$	$0.34^{+0.15}_{-0.07}$	$2.28^{+1.01}_{-1.03}$	38.8/32	99.9
Mrk 78 ^d
Mrk 273	$1.88^{+0.50}_{-0.88}$	$0.35^{+0.14}_{-0.15}$	$0.41^{+0.36}_{-0.15}$	$0.35 < 0.69$	13.6/17	99.5

NOTE.—The Raymond-Smith abundance was fixed at solar.

^a Normalization in units of 10^{-4} photons $\text{cm}^{-2} \text{s}^{-1} \text{keV}^{-1}$ at 1 keV.

^b The F -test indicating the significance of the improvement on addition of the Raymond-Smith component to the model, vs. the fits in Table 5.

^c The fit would not converge unless the Raymond-Smith temperature was fixed (we used the mean temperature from fits to other sources).

^d The fit did not find a unique solution, due to the low signal-to-noise ratio in these data.

trum of Mrk 3 (Miller & Goodrich 1990), consistent with this picture. The BBXRT observation ($\sim 1\text{--}10$ keV) shows the same highly absorbed power-law spectrum as *Ginga* (Marshall et al. 1991), while the soft spectrum is well modeled by a steep power law of $\Gamma \sim 3$, or a 90 eV blackbody, absorbed only by the Galactic line-of-sight column.

The *ROSAT* data show a heavily absorbed steep soft excess component (Table 4). When the absorption is fixed at the Galactic value (Table 5), the fit is much worse, showing either that the soft X-ray component is significantly absorbed by material intrinsic to the source, or that a more complex model is required. The absorption observed in the *ROSAT* bandpass (Table 4), however, is two orders of magnitude lower than that implied for the hard component (from the *Ginga* and BBXRT data). Natural explanations for the discrepancy between the two bandpasses include the following:

1. Partial covering of the source by the absorber. Marshall et al. (1991) show that the BBXRT observations require $\sim 3\%$ of the absorbed component to be uncovered or scattered.
2. Spectral variability.
3. Ionized absorbing material. This would have a reduced opacity in the PSPC bandpass compared to the *Ginga* and BBXRT bandpasses.
4. The soft component suffers only extinction due to the host galaxy.

The residuals to the simple absorbed power-law fits of Tables 4 and 5 (Fig. 4) suggest a more complex model is required for the soft X-ray spectrum. When an emission line is added to the model, the fit to the mean spectrum is improved dramatically (99.9% confidence) for a line of energy 0.78 keV and equivalent width 333 eV; the underlying photon index is flattened to $\Gamma = 2.26$. The energy of the line (or line blend) suggests an origin as iron L and oxygen K emission lines from ionized material, possibly associated with the active nucleus. When the excess is modeled as a Raymond-Smith equilibrium plasma, the best-fit temperature is 0.34 keV. The relatively low signal-to-noise ratio of the spectral data meant we could not set any interesting constraints on the emission line variability.

4.5. Mrk 78

Mrk 78 was first observed in the optical regime by Adams (1973), he noted two distinct emission line components in the nucleus. De Robertis (1987) suggested the eastern nuclear component to be the nucleus of a companion galaxy. The *ROSAT* PSPC observation shows that the field is obviously very rich in X-ray sources of a comparable flux to Mrk 78 (Fig. 1*f*). Again, this illustrates that source confusion has been important in previous X-ray measurements. The closest sources to Mrk 78 are shown in Figure 1*f*; none of these have identified optical counterparts in the literature, and potential identifications of the sources are discussed in § 3.1.3. The discovery of these serendipitous sources means that the previous claim of flux variability in Mrk 78 (Urry et al. 1986) may have been attributable to variability in one of the sources close to Mrk 78 (which would have been unresolvable with the *Einstein* IPC). Mrk 78 was not detected by *Ginga*, and the upper limit on the flux is given as a soft/hard ratio in Table 4. The *Einstein* IPC spectrum is flat and unabsorbed with $\Gamma = 1.45$ and $N_{\text{H}} \sim 8 \times 10^{19}$ cm $^{-2}$, while the PSPC spectrum is steeper and more heavily absorbed. The constraints on the IPC and PSPC spectral parameters are very poor, however; thus, no interesting con-

straints can be obtained on the spectral variability of this source.

4.6. Mrk 273

This galaxy is known to be extremely luminous in the infrared bandpass. Markarian (1969) noted the 20 kpc jet or protrusion to the southwest. Sanders et al. (1988) discuss some of the sources in the vicinity of Mrk 273, and the companion X-ray source in the PSPC data (Fig. 1*g*) is coincident with an optical source in their figure. That source is not identified in their paper, however, or anywhere else in the literature. While the optical "jet" is thought to be related to merger activity in the system, the merger candidate is a very close infrared source (not detected in the PSPC data). Potential identifications for the X-ray source are discussed in § 3.1.3.

5. DISCUSSION

Our *ROSAT* PSPC observations of six Seyfert 2 galaxies have produced unexpected results in each of the three areas explored: spatial timing, and spectral analysis. In each field, serendipitous sources are found near the target source. Averaged over all seven fields, there is a statistically significant excess of nearby sources compared to surface densities in the same fields (but farther away from the target source) and compared to the predicted source density from deep survey data (Branduardi-Raymont et al. 1993). Estimates of optical-to-X-ray flux ratios suggest that some of these are likely to be extragalactic, but follow-up optical spectroscopy is needed to unambiguously identify the new X-ray sources. Given the surface density of AGNs and clusters of galaxies on the sky, some of the serendipitous sources may be physically associated with the target Seyfert 2 galaxies. In NGC 1365, the serendipitous sources seem most likely to be high-luminosity X-ray binary systems within the host galaxy. In any case, the proximity of these serendipitous sources to the target sources has probably confused previous, lower spatial resolution X-ray observations, and illustrates how important source confusion is on a 1' scale for these objects.

Observations typically contained $\sim 12,000$ s of good data and count rates were in the range 0.01–0.27 counts s $^{-1}$. We were able to search for variability on timescales of several minutes (within each observation interval [OBI]) and on timescales of a half-day to several days (between the OBIs). Rapid soft X-ray variability is not expected in the unified model, as direct view of the active nucleus of a Seyfert 2 galaxy should be obscured and the scattering region is large. Significant rapid variability was observed in Mrk 372 and NGC 1365. The soft X-ray luminosity of Mrk 372 is more typical of a Seyfert 1 galaxy than a Seyfert 2, and its optical spectrum has shown some broad lines, suggesting that this source is relatively unobscured at the present epoch, allowing direct observation of variations in the nuclear source. In NGC 1365 the fluctuations may be due to variability in the serendipitous sources (which are so close that their source counts cannot be entirely deconvolved from those arising in the active nucleus); thus, these observations of soft X-ray variability do not pose a problem for the unified model.

The luminosities observed in the *ROSAT* bandpass are a factor of 10–100 lower than those of Seyfert 1 galaxies. If Seyfert 2 galaxies were intrinsically less luminous sources, then one would expect them to be comparably less luminous in the hard X-ray regime. Those Seyfert 2 galaxies detected in the hard X-ray regime, however, appear to have comparable hard

X-ray luminosities to Seyfert 1 galaxies (Awaki et al. 1991; Marshall et al. 1991), but the majority of Seyfert 2 galaxies have not been detected as hard X-ray sources. It seems likely that some Seyfert 2 galaxies are simply low-luminosity AGNs in the hard and soft X-ray regimes, while others are Seyfert type 1 nuclei heavily obscured in our line of sight, for which we see a scattered soft X-ray component.

The present data provide new information on the X-ray spectra of Seyfert 2 galaxies since the typical *Einstein* IPC observations were shorter, less sensitive, and had less spectral resolution than the *ROSAT* PSPC. The observed spectra tend to be steep when fitted with an absorbed power-law model, compared to Seyfert 1 galaxies or Seyfert 2 spectra seen with the IPC. The latter may in part be due to the softer response of the PSPC. Analysis of the higher signal-to-noise ratio PSPC observations suggests that the apparent steepness may be due to the presence of unresolved, high equivalent width, iron and oxygen line emission in the spectra in the 0.7–0.85 keV range (we note that this is somewhat speculative as the statistical constraints presented here are very weak, but the speculation is strengthened by the observation that Seyfert 2 galaxies do show higher equivalent width iron K lines in hard X-ray *Ginga* and *BBXRT* data; e.g., Marshall et al. 1991; Awaki et al. 1991). The high equivalent widths of the emission lines are expected in the unified model, because the equivalent width of the line is measured against the scattered continuum rather than the ionizing continuum (Krolik & Kallman 1987; Band et al. 1990). Finally we note (again) that it is not possible to unambiguously interpret the spectral complexity observed in these data; *ASCA* observations are required to distinguish between various plausible models.

The transition behavior (changes in optical spectral properties) observed in Mrk 372 (and other sources in the literature) implies that (in the unified model) variations occur in the amount or state of the material obscuring the broad line region. The unified model proposes that the obscuring material is in the form of a molecular torus. In the case of a source like Mrk 372, a variable ionization state could affect the dust content of the absorber by destroying dust grains at high ion-

ization states, leading to changes in the $H\beta/H\alpha$ ratio. Alternatively, if the absorber were in the form of molecular clouds, variable absorption would be possible as clouds moved across the line-of-sight. Variable X-ray absorption has been observed in sources intermediate in optical characteristics between Seyfert type 1 and 2 nuclei. For example, in ESO 103-G55, although the column is very large, significant variability has been observed between the *EXOSAT* observations (Warwick, Pounds, & Turner 1988).

6. CONCLUSIONS

The PSPC data show an excess of serendipitous sources within a few arcminutes of the Seyfert 2 galaxies presented in this paper. In NGC 1365 these appear to be luminous X-ray binaries in the host galaxy. These observations illustrate that source confusion can be very important on a 1' scale for Seyfert 2 galaxies.

There is evidence for complexity of the source spectra, most notably in Mrk 3 and NGC 1365. The data are suggestive of the presence of high equivalent width soft X-ray line emission, probably dominated by iron L and ionized oxygen emission.

Significant flux variability is observed in Mrk 372 and NGC 1365. Mrk 372 appears in all respects to be a low-luminosity Seyfert 1 galaxy at this epoch, and we are probably seeing variations in the unobscured nuclear continuum source. In NGC 1365 the variable nearby serendipitous sources may contribute to the observed variability.

The authors would like to thank Krista Lawrance, Kip Kuntz, Anne Gonnella, and Daniel Golombek for help with the optical identifications using the GASP system. We thank Rem Stone, Matt Malkan, and Brian Rush for useful discussions related to the optical counterparts of the serendipitous X-ray sources; we thank Rick Shafer for useful discussions on statistics; and we thank the referee for some very constructive comments. This work made use of the NASA/IPAC Extragalactic database (NED) and the online HEASARC database.

REFERENCES

- Adams, T. F. 1973, *ApJ*, 179, 417
 Alloin, D., Edmunds, M. G., Lindblad, P. O., & Pagel, B. E. J. 1981, *A&A*, 101, 377
 Antonucci, R. R. J., & Miller, J. S. 1985, *ApJ*, 297, 621
 Arakelian, M. A., Dibay, E. A., & Yesipov, V. F. 1972, *Astrofizika*, 8, 177
 Awaki, H., Koyama, K., Inoue, H., & Halpern, J. P. 1991, *PASJ*, 43, 195
 Awaki, H., Koyama, K., Kunieda, H., & Tawara, Y. 1990, *Nature*, 346, 544
 Band, D. L., Klein, R. I., Castor, J. I., & Nash, J. K. 1990, *ApJ*, 362, 90
 Branduardi-Raymont, G., et al. 1993, *MNRAS*, submitted
 Code, A., et al. 1991, *BAAS*, 23, 971
 De Robertis, M. M. 1987, *ApJ*, 316, 597
 Elvis, M., & Lawrence, A. 1988, *ApJ*, 331, 161
 Elvis, M., Maccacaro, T., Wilson, A. S., Ward, M. J., Penston, M. V., Fosbury, R. A. E., & Perola, G. C. 1978, *MNRAS*, 183, 129
 Fabbiano, G., Kim, D., & Trinchieri, G. 1992, *ApJS*, 80, 531
 Gregory, S. A., Tift, W. G., & Cocke, W. J. 1991, *AJ*, 102, 1978
 Gioia, I. M., Henry, J. P., Maccacaro, T., Morris, S. L., Stocke, J. T., & Wolter, A. 1990, *ApJ*, 356, L35
 Hasinger, G., & Snowden, S. 1990, MPE note, Calibration Corrections to Individual Events
 Hasinger, G., Turner, T. J., George, I. M., & Boese, G. 1992, *Legacy*, 2, 77 (OGIP Calibration Memo CAL/ROS/92-001)
 Kinney, A. L., Antonucci, R. R. J., Ward, M. J., Wilson, A. S., & Whittle, M. 1991, *ApJ*, 377, 100
 Koski, A. 1978, *ApJ*, 223, 56
 Koyama, K., Inoue, H., Tanaka, Y., Awaki, H., Ohashi, T., & Matsuoka, M. 1989, *PASJ*, 41, 731
 Kriss, G. A., Canizares, C. R., & Ricker, G. R. 1980, *ApJ*, 242, 492
 Krolik, J. H., & Kallman, T. 1987, *ApJ*, 320, L5
 Kruper, J. S., Urry, C. M., & Canizares, C. R. 1991, *ApJS*, 74, 347
 Kuerster, M., & Hasinger, G. 1992, TN-ROS-ME-ZA00/028
 Lampton, M., Margon, B., & Bowyer, S. 1976, *ApJ*, 208, 177
 Lawrence, A., & Elvis, M. 1982, *ApJ*, 256, 410
 Maccacaro, T., Perola, G. C., & Elvis, M. 1982, *ApJ*, 257, 47
 Markarian, B. E. 1969, *Astrofizika*, 5, 443
 Marshall, F., et al. 1991, in *Frontiers of X-ray Astronomy, Proc. 28th Yamada Meeting*, ed. Y. Tanaka & K. Koyama (Tokyo: Universal Academy), 221
 Miller, J. S., & Goodrich, R. W. 1990, *ApJ*, 355, 456
 Monier, R., & Halpern, J. P. 1987, *ApJ*, 315, L17
 Osmer, P. S., Smith, N. G., & Weedman, D. W. 1974, *ApJ*, 192, 279
 Penston, M. V., & Perez, E. 1984, *MNRAS*, 211, 33P
 Pfeffermann, E. et al. 1986, in *Soft X-Ray Optics and Technology (Proc. SPIE 733)*, 519
 Rowan-Robinson, M. 1977, *ApJ*, 213, 638
 Sanders, D. B., Soifer, B. T., Elias, J. H., Madore, B. F., Matthews, K., Neugebauer, G., & Scoville, N. Z. 1988, *ApJ*, 325, 74
 Stark, A. A., Heiles, C., Bally, J., & Linke, R. 1993, in preparation
 Stocke, J. T., Morris, S. L., Gioia, I. M., Maccacaro, T., Schild, R., Wolter, A., Fleming, T. A., & Henry, J. P. 1991, *ApJS*, 76, 813
 Tananbaum, H., Peters, G., Forman, W., Giacconi, R., & Jones, C. 1978, *ApJ*, 223, 74
 Tran, H. D., Miller, J. S., & Kay, L. E. 1992, *ApJ*, 397, 452
 Truemper, J. 1983, *Adv. Space. Res.*, 2, 241
 Turner, T. J., George, I. M., & Mushotzky, R. F. 1993, *ApJ*, 412, 72

- Turner, T. J., & Pounds, K. A. 1989, MNRAS, 240, 833
- Urry, C. M., Arnaud, K., Edelson, R. A., Kruper, J. S., & Mushotzky, R. F. 1989, in AGN and the X-Ray Background, ed. N. White (Paris: ESA), 789
- Urry, C. M., Kruper, J. S., Canizares, C. R., Rohan, M. L., & Oberhardt, M. R. 1986, in Variability of Galactic and Extragalactic X-Ray Sources, ed. A. Treves (Milan: Assoc. per L'Avanzamento dell'Astronomia), 15
- Véron-Cetty, M. P., & Véron, P. 1989, A Catalogue of Quasars and Active Galactic Nuclei (3d ed.; Garching: ESO)
- Wagner, S. J., & Anton, K. 1989, in Proc. of the ESO Workshop on Extranuclear Activity in Galaxies, ed. E. J. A. Meurs & R. A. E. Fosbury (Garching: ESO), 195
- Warwick, R. S., Pounds, K. A., & Turner, T. J. 1988, MNRAS, 231, 1145
- Wilson, A. S., Elvis, M., Lawrence, A., & Bland-Hawthorn, J. 1992, ApJ, 391, L75